



Effects of encapsulation elasticity on the stability of an encapsulated microbubble

Amit Katiyar, Kausik Sarkar*, Pankaj Jain

Mechanical Engineering Department, University of Delaware, 126, Spencer Lab, Newark, DE 19716, USA

ARTICLE INFO

Article history:

Received 27 February 2009

Accepted 6 May 2009

Available online 18 May 2009

Keywords:

Microbubble
Ultrasound contrast agents
Dissolution
Stability
Permeability
Surface tension
Encapsulation
Interfacial elasticity

ABSTRACT

A model for gas transport from an encapsulated microbubble into the surrounding medium is developed and investigated incorporating the effects of encapsulation elasticity. Encapsulation elasticity stabilizes microbubbles against dissolution and explains the long shelf life of microbubble contrast agent. We consider air bubbles as well as bubbles containing perfluorocarbon gas. Analytical conditions between saturation level, surface tension and interfacial dilatational elasticity are determined for attaining non-zero equilibrium radius for these microbubbles. Numerical solution of the equation verifies the stability of the equilibrium radii. In an undersaturated medium all encapsulated bubbles dissolve. In a saturated medium, an encapsulated bubble is found to achieve a long-time stable radius when interfacial dilatational elasticity is larger than equilibrium surface tension. For bubbles with interfacial dilatational elasticity smaller than the equilibrium surface tension, stable bubble of non-zero radius can be achieved only when the saturation level is greater than a critical value. Even if they initially contain a gas other than air, bubbles that reach a stable radius finally become air bubbles. The model is applied to an octafluoropropane filled lipid-coated 2.5 μm bubble, which displayed a transient swelling due to air intake before reaching an equilibrium size. Effects of elasticity, shell permeability, initial mole fraction, initial radius and saturation level are investigated and discussed. Shell permeability and mole fraction do not affect the final equilibrium radius of the microbubble but affect the time scale and the transient dynamics. Similarly, the ratio of equilibrium radius to initial radius remains unaffected by the variation in initial radius.

© 2009 Elsevier Inc. All rights reserved.

1. Introduction

Gas filled micron-size bubbles are intravenously injected in patients as contrast improving agents for diagnostic ultrasound imaging and for drug delivery [1–9]. Free air bubbles of such small size dissolve in water in milliseconds [10]. Contrast microbubbles are stabilized by encapsulating them with a layer of lipids (SonoVue, Definity, and Sonazoid), proteins (human serum albumin for Optison), and surfactants (SonoRx, Imavist). Epstein and Plesset developed an analytical model for bubble dissolution and investigated the effects of surface tension and saturation level of the surrounding liquid [11]. The pressure inside the bubble exceeds the external pressure by the surface tension induced Laplace pressure; higher pressure leads to higher gas concentration driving outward diffusion. Using less soluble perfluorocarbon instead of air and the encapsulation lead to much longer shelf life for contrast microbubbles [3,10].

An encapsulation stabilizes a bubble by various mechanisms; Wang et al. suggested three—reduced surface tension, increased resistance to gas permeation and surface hardening [12,13]. The first two effects have been modeled [10]. But effects of surface hardening, more precisely encapsulation elasticity, on stability

against dissolution of encapsulated contrast microbubbles have not been investigated. It is curious to note that almost all models for encapsulation of contrast microbubbles assume it to be elastic. Encapsulation elasticity increases the spring constant of the oscillating bubble and thereby increases its resonance frequency. Consequently, resonance radius as well as scattering and attenuation cross-sections are affected, leading to major impact on overall contrast achieved by any microbubble contrast agent [1,14–22]. In this paper we investigate the effects of encapsulation elasticity on stability of encapsulated microbubbles.

The effects of surface tension on bubble dissolution as described by the Epstein–Plesset model was recently subjected to a careful experimental test by Duncan and Needham [23]; they directly observed dissolution of a lipid-shelled bubble of radius 15 μm supported on a micropipette and found the model to be accurate within 10%. For impeded gas permeability through the encapsulation, Borden and Longo assumed extra resistance terms due to a lipid monolayer and a PEG layer in the bubble dissolution model [3,13]. The model was compared with experimental observation of dissolution of a 25 μm lipid coated air bubble to infer a value of ~ 100 –500 s/cm for the shell resistance depending on hydrophobic chain length in the lipid. We have recently developed a detailed mathematical model of gas permeation through the encapsulating shell and investigated the effects of surface tension and shell permeability on dissolution of an encapsulated contrast microbubble

* Corresponding author. Fax: +1 302 831 3619.

E-mail address: sarkar@udel.edu (K. Sarkar).

[10]. The model was then used to describe the behavior of a contrast microbubble similar to Definity using realistic material properties. We showed that such a microbubble before dissolving experiences transient growth due to intake of air dissolved in the surrounding medium. It explains our previous experimental observations of transient increase in attenuation in Definity [24] as well as similar observations by other groups [25–27]. More importantly for the present work, we found that even though low permeability slows down bubble dissolution, for realistic parameters, bubble life time of more than an hour is only possible with surface tension lower than 1 mN/m. On the other hand, contrast agents are known to have long self-life up to one year [28]. Here we show that shell elasticity has an additional stabilizing effect leading to long-lasting stable bubbles. It should be noted that there have been prior modeling studies of stabilizing effects of surface elasticity on bubbles, but not specifically for contrast microbubbles. In the seventies, Yount surmised an elastic skin of surface active materials on bubbles occurring in tap water and sea [29]. He investigated static equilibrium of forces and showed that the surface pressure may counter Laplace pressure impeding dissolution. Recently, Kloek et al. performed a theoretical study of effects of interfacial and bulk viscosity and elasticity on bubbles arising in aerated food products [30]. They found that the viscosity only retards bubble dissolution, but appropriate elasticity can stop it.

In our presentation, we briefly describe the mathematical formulation of the gas transport from an encapsulated bubble using an Epstein–Plesset model but modified for the permeability barrier due to encapsulation [10]. We use an interfacial rheological model for the encapsulation with a dilatational elasticity term [19]. We discuss the static equilibrium radius for an encapsulated bubble. We investigate a model contrast microbubble having properties representative of contrast agent Definity; it has a lipid encapsulation and contains octafluoropropane (OFP). Material properties such as diffusivities, Ostwald coefficients of air and octafluoropropane were determined from the literature. Presence of octafluoropropane inside and air dissolved in the surrounding medium is modeled. We finally discuss the effects of various relevant properties such as permeability, initial bubble radius, and initial mole fraction of OFP on bubble growth and stability. The final section summarizes our findings.

2. Mathematical formulation

We have discussed in detail the gas transport in the medium surrounding an encapsulated bubble in a recent paper [10]. Here we briefly describe the mathematical equations for the sake of completeness. We neglect convection and the unsteady effects (time scale of dissolution is much larger than the time scale of gas transport R_0/h_g , where R_0 is the initial bubble radius and h_g is the permeability of gas through the membrane). The governing equation for gas concentration C in the surrounding medium and the boundary conditions (at the outer surface of the encapsulation and far away from the bubble) are

$$\frac{1}{r^2} \frac{\partial}{\partial r} \left(r^2 \frac{\partial C}{\partial r} \right) = 0, \quad -k_g \frac{\partial C}{\partial r} \Big|_R = h_g [C_w - C(R)], \quad C(r \rightarrow \infty) = C_\infty, \quad (1)$$

where R is the bubble radius, h_g is permeability of the gas through the encapsulation, k_g is the diffusivity in the surrounding liquid, C_w is the gas concentration at the inside wall of the encapsulation, and C_∞ is the gas concentration far from the bubble. As has been discussed previously [10], the linear model of permeability is appropriate for both classical Fickian diffusion as well as an energy barrier model that might be more appropriate for a monolayer [13,31]. One solves (1) to obtain

$$C(r) = \frac{R^2 (C_w - C_\infty)}{r \left(\frac{k_g}{h_g} + R \right)} + C_\infty. \quad (2)$$

Using mass conservation at concentration C_g inside the bubble, one obtains

$$\frac{d(R^3 C_g)}{dt} = 3R^2 k_g \frac{(C_\infty - L_g C_g)}{\left(\frac{k_g}{h_g} + R \right)}, \quad (3)$$

where we have assumed that the gas concentration at the inner wall of the membrane C_w is directly related to the inside gas concentration by the Ostwald coefficient (L_g) as $C_w = L_g C_g$. Far from the bubble concentration $C_\infty = f L_g p_{\text{atm}} / R_G T$. p_{atm} is the atmospheric pressure and R_G is the universal gas constant. The factor f describes whether the liquid is saturated ($f = 1$), undersaturated ($f < 1$) or oversaturated ($f > 1$) with the gas.

2.1. Elastic stabilization of single gas encapsulated bubble

The pressure inside the bubble exceeds the outside pressure by the Laplace pressure due to surface tension γ :

$$p_g = C_g R_G T = p_{\text{atm}} + \frac{2\gamma(R)}{R}. \quad (4)$$

The elasticity is modeled using a Gibbs elasticity type constitutive model, where a dilatational surface elasticity E^s term appears as derivative of surface tension with respect to fractional change in interfacial area [19]

$$E^s = \frac{d\gamma}{dA/A_0},$$

$$\gamma(R) = \begin{cases} \gamma_0 + E^s \left[\left(\frac{R}{R_0} \right)^2 - 1 \right], & \text{for } \gamma_0 + E^s \left[\left(\frac{R}{R_0} \right)^2 - 1 \right] > 0, \\ 0, & \text{for } \gamma_0 + E^s \left[\left(\frac{R}{R_0} \right)^2 - 1 \right] \leq 0. \end{cases} \quad (5)$$

Here we assume that the initial radius R_0 corresponds to a stress-free conformation: $R_0 = R_E$. $\gamma_0 \equiv \gamma(R_0)$ is the surface tension at that radius value. If the bubble radius increases from the stress-free value, surface tension increases; the increased tension at the interface tries to bring the surface back to the stress-free conformation. On the other hand, if the bubble radius is smaller than the stress-free value, the second term in (5) is negative, and the compression results in a stress trying once again to bring the radius back to the stress-free value. Note that as the radius changes,

$$\left. \begin{aligned} \gamma(R) &> 0, & \text{for } E^s/\gamma_0 \leq 1 \\ \gamma(R) &> 0, \text{ for } R > R_s \\ \gamma(R) &= 0, \text{ for } R \leq R_s \end{aligned} \right\}, \text{ for } E^s/\gamma_0 > 1, \text{ where } R_s = R_0(1 - \gamma_0/E^s)^{1/2}. \quad (6)$$

We have imposed a restriction $\gamma(R) \geq 0$. For $\gamma(R) < 0$ the surface could be in a compressive state which will lead to buckling [32]. Note that although elasticity is introduced here through surface tension variation, one can very well take γ_0 and E^s to be independent constitutive parameters. For a more solid interface, such a physical model could be more appropriate (see discussion below).

Using Eqs. (4) and (5) and value of $C_\infty = f L_g p_{\text{atm}} / R_G T$, we find from Eq. (3):

$$\frac{dR}{dt} = \frac{-3L_g k_g}{\left(\frac{k_g}{h_g} + R \right)} \left[\frac{p_{\text{atm}}(1-f) + \frac{2\gamma}{R}}{3p_{\text{atm}} + \frac{4\gamma}{R} + 2\frac{d\gamma}{dR}} \right]. \quad (7)$$

As was underscored by Epstein and Plesset, Eq. (7) clearly shows that the bubble is driven to dissolution by surface tension and undersaturation ($f < 1$). Replacing air with a sparingly soluble gas

(lower L_g) would lead to a longer shelf-life for contrast microbubbles. Also very low permeability (low h_g) through encapsulation would result in enhanced microbubble stability. Both methods of stabilization are employed for commercial contrast microbubbles—encapsulating it with surface active molecules and replacing air by perfluorocarbon.

Note that $d\gamma/dR$ is discontinuous at $R = R_0(1 - \gamma_0/E^s)^{1/2}$ from Eq. (6). Therefore Eq. (7) becomes

$$\frac{dR}{dt} = \frac{-3L_g k_g}{\left(\frac{k_g}{h_g} + R\right)} \left[\frac{p_{\text{atm}}(1-f) + \frac{2\gamma_0}{R} + \frac{2E^s}{R} \left\{ \left(\frac{R}{R_0}\right)^2 - 1 \right\}}{3p_{\text{atm}} + \frac{4\gamma_0}{R} + \frac{4E^s}{R} \left\{ 2\left(\frac{R}{R_0}\right)^2 - 1 \right\}} \right],$$

for $\gamma(R) = \gamma_0 + E^s \left[\left(\frac{R}{R_0}\right)^2 - 1 \right] > 0$, (8)

$$\frac{dR}{dt} = \frac{-L_g k_g}{\left(\frac{k_g}{h_g} + R\right)} (1-f), \quad \text{for } \gamma(R) = 0.$$

Eq. (8) reduces to the familiar Epstein–Plesset form in absence of encapsulation ($h_g \rightarrow \infty$, $E^s \rightarrow 0$, or more appropriately in terms of non-dimensional numbers $h_g R_0/k_g \rightarrow \infty$, $E^s/(p_{\text{atm}} R_0) \rightarrow 0$) [11]. Non-dimensionalizing Eq. (8), we get for $R = R/R_0$ as a function of $\tau = tk_g/R_0^2$

$$\frac{d\widehat{R}}{d\tau} = \frac{-3L_g}{(\alpha_g + \widehat{R})} \left[\frac{\widehat{R}(1-f) + \widehat{\gamma} + \widehat{E} \left\{ \widehat{R}^2 - 1 \right\}}{3\widehat{R} + 2\widehat{\gamma} + 2\widehat{E} \left\{ 2\widehat{R}^2 - 1 \right\}} \right], \quad \text{for } \widehat{\gamma} + \widehat{E} \left\{ \widehat{R}^2 - 1 \right\} > 0,$$

$$\frac{d\widehat{R}}{d\tau} = \frac{-3L_g}{(\alpha_g + \widehat{R})} \left[\frac{\widehat{R}(1-f)}{3\widehat{R}} \right], \quad \text{for } \widehat{\gamma} + \widehat{E} \left\{ \widehat{R}^2 - 1 \right\} \leq 0, \quad (9)$$

respectively, where $\alpha_g = k_g/(h_g R_0)$, $\widehat{\gamma} = 2\gamma_0/(p_{\text{atm}} R_0)$ and $\widehat{E} = 2E^s/(p_{\text{atm}} R_0)$. Eq. (9) is numerically solved with the initial condition $R(\tau = 0) = 1$ using MATLAB-R2007b (The MathWorks Inc., Natick, MA, USA). Using the non-dimensional form (9) instead of (8) aids in numerical solution. Matlab subroutine ODE15s appropriate for stiff differential equation is used. Solution requires a user defined function that provides the right-hand side of Eq. (9). Simulated results have been checked for their independence of the various option parameters (viz. absolute and relative tolerance values) of the solver.

It is evident from Eq. (8) that undersaturation ($f < 1$) results in eventual bubble dissolution. In a saturated ($f = 1$) medium, a non-zero equilibrium bubble radius is reached if only the interfacial tension γ_0 is counterbalanced by the encapsulation elasticity giving $\gamma(R) = 0$ and correspondingly $dR/dt = 0$ in Eq. (8):

$$R_{\text{equilibrium}} = R_s = R_0(1 - \gamma_0/E^s)^{1/2} \quad \text{for } f = 1 \quad \text{and } E^s > \gamma_0. \quad (10)$$

On the other hand, strong enough oversaturation ($f > 1$) can overcome interfacial tension resulting in a nonzero equilibrium radius:

$$R_{\text{equilibrium}} = R_0 \left[\varepsilon + \sqrt{\varepsilon^2 + \left(1 - \frac{\gamma_0}{E^s}\right)} \right], \quad \text{for } f > 1 \quad \text{and } E^s \geq \gamma_0, \quad (11)$$

$$\left. \begin{aligned} R_{\text{equilibrium}}^{(1)} &= R_0 \left[\varepsilon + \sqrt{\varepsilon^2 + \left(1 - \frac{\gamma_0}{E^s}\right)} \right] \\ R_{\text{equilibrium}}^{(2)} &= R_0 \left[\varepsilon - \sqrt{\varepsilon^2 + \left(1 - \frac{\gamma_0}{E^s}\right)} \right] \end{aligned} \right\}$$

for $f \geq 1 + \frac{4}{P_{\text{atm}} R_0} \sqrt{E^s(\gamma_0 - E^s)}$ and $E^s < \gamma_0$, (12)

where $\varepsilon = \frac{R_0 p_{\text{atm}}(f-1)}{4E^s}$.

For $E^s < \gamma_0$, we have two possible equilibrium solutions, however, by solving Eq. (8) numerically, we would see below that $R_{\text{equilibrium}}^{(2)}$ is not realized dynamically indicating that it is an unstable equilibrium. A slight perturbation would drive the system away from it.

2.2. Effects of multiple gases

For the case of a microbubble contrast agent containing a gas other than air (e.g. perfluorocarbon), diffusion of both gases, air (A) and perfluorocarbon (F), has to be considered. Far from the bubble, perfluorocarbon concentration $C_F(\infty)$ is zero, whereas air concentration is as before $C_A(\infty) = fL_A p_{\text{atm}}/R_G T$. We get two equations for the two gases from (3) [10,33]:

$$\frac{d(R^3 C_F)}{dt} = -3Rk_F \frac{L_F C_F}{\left(\frac{k_F}{h_F} + 1\right)}, \quad (13)$$

$$\frac{d(R^3 C_A)}{dt} = 3Rk_A L_A \frac{\left(f \frac{p_{\text{atm}}}{R_G T} - C_A\right)}{\left(\frac{k_A}{h_A} + 1\right)}. \quad (14)$$

The pressure balance across the gas–liquid interface obtains:

$$p_A + p_F = (C_A + C_F)R_G T = p_{\text{atm}} + \frac{2\gamma(R)}{R}. \quad (15)$$

Multiplying Eq. (15) by R^3 and differentiating with respect to t , and using Eqs. (13) and (14) we obtain an equation for $R(t)$

$$\frac{dR}{dt} = \frac{R_G T}{R^2 \left(3p_{\text{atm}} + \frac{4\gamma}{R} + 2\frac{d\gamma}{dR}\right)} \left[\frac{d(R^3 C_A)}{dt} + \frac{d(R^3 C_F)}{dt} \right]. \quad (16)$$

Introducing initial mole-fraction of the perfluorocarbon (X_F):

$$X_F = \frac{C_F(0)}{C_A(0) + C_F(0)}. \quad (17)$$

We obtain initial conditions:

$$\begin{aligned} C_F(0) &= X_F \left(\frac{p_{\text{atm}}}{R_G T} + \frac{2\gamma_0}{R_0 R_G T} \right), \\ C_A(0) &= (1 - X_F) \left(\frac{p_{\text{atm}}}{R_G T} + \frac{2\gamma_0}{R_0 R_G T} \right). \end{aligned} \quad (18)$$

Looking for equilibrium solution, we notice from Eq. (13) that $C_F(t \rightarrow \infty) \rightarrow 0$. Therefore, the equilibrium solution will be the same as that for the single gas bubble, Eqs. (10)–(12), with the gas being air. Indeed, when $C_F \rightarrow 0$, one obtains the same Eq. (7) from Eq. (16). Even though the bubble initially contains perfluorocarbon, with time it will diffuse out of the bubble. Depending on the level of saturation f and E^s/γ_0 eventually an air bubble will either reach a non-zero radius or dissolve away. However, the transient dynamics will be different because of the presence of the perfluorocarbon gas, and will be determined numerically by solving Eqs. (13), (14) and (16) using initial conditions (18).

3. Results and discussion

For a numerical investigation of our model we use a bubble similar in properties to that of the contrast agent Definity as in our previous study [10]. It has a narrow radius distribution with a mean diameter of 2.5 μm , and contains octafluoropropane (OFP; $n\text{-C}_3\text{F}_8$) [34,35]. The encapsulation is made of a mixture of three different lipids: DPPA ((R)-hexadecanoic acid, 1-[(phosphonoxy)methyl]-1,2-ethnediyl ester, monosodium salt), DPPC ((R)-4-hydroxy-*N,N,N*-trimethyl-10-oxo-7-[(1-oxohexadecyl)-oxy]-3,4,9-trioxo-4-phosphapentacosan-1-aminium, 4-oxide, inner

Table 1
Physical properties used in simulations.

Initial bubble radius (R_0)	1.25×10^{-6} m
Atmospheric pressure (p_{atm})	101,325 Pa
Coefficient of diffusivity of air in water (k_A)	2.05×10^{-9} m ² s ⁻¹
Coefficient of diffusivity of air (k_F)	7.45×10^{-10} m ² s ⁻¹
Surface tension (γ_0)	0.025 mN/m
Ostwald coefficient of OFP (L_F)	5.2×10^{-4}
Ostwald coefficient of OFP (L_A)	1.71×10^{-2}
Permeability of air through the encapsulation (h_A)	2.857×10^{-5} m s ⁻¹
Permeability of OFP through the encapsulation (h_F)	1.2×10^{-6} m s ⁻¹

salt), and MPEG5000 DPPE ((R)- α -[6-hydroxy-6-oxido-9-[(1-oxohexadecyl)oxy]-5,7,11-trioxa-2-aza-6-phosphahexacos-1-yl]- ω -methoxypoly(ox-1,2-ethanediyl), monosodium salt). Property values used for the simulation are obtained from the chemical literature as discussed in [10], and presented in Table 1. The rheological properties of the encapsulation such as surface tension and surface elasticity are difficult to determine for a micron-size bubble. We have developed an acoustic characterization method using measurement of attenuation of ultrasound through an emulsion of contrast agent [18,19]. Here we assume the interfacial tension to be 0.025 N/m as found for a liquid phase lipid monolayer [23]. (For a waxy solid lipid layer zero interfacial tension has been reported [23,36].) The permeabilities of air and OFP ($h_{A,F}$) through encapsulation in Table 1 are determined using energy barrier model that depends on gas molecules' collision diameter and the surface pressure [10,37–40]. Using 1 nm encapsulation thickness and bulk lipid diffusivity of 10^{-14} m²/s gives a permeability value of the same order ($h_g \approx 10^{-5}$ m/s) even for a Fick's type model [13].

3.1. Value of surface dilatational elasticity

As noted above determining surface dilatational elasticity is difficult. It depends on the nature of the interface; just like a bulk material, the interface can be in gaseous, liquid or solid states with co-existing phases and possibilities of undergoing phase transitions [36,40]. As was mentioned in the introduction, early on elasticity of encapsulation was recognized to modify the contrast properties of agents. Indeed the resonance frequency of a contrast microbubble is larger than that of a free bubble of the same radius due to the elasticity of the encapsulation (elasticity contributes to the spring constant of the bubble oscillator). Several models have been developed to describe the effects of encapsulation elasticity. We introduced interfacial rheological model for an encapsulation with interfacial dilatational elasticity (5), and acoustically determined its value, $E^s = 0.51$ N/m, for lipid-coated contrast microbubble Sonazoid [19]. An elegant physical description of the surface Gibbs elasticity arising from interfacial tension variation was provided by Marmottant et al. with essentially the same equation in the linear region [41]. They estimated same order of value for elasticity, $E^s = 1$ N/m by fitting a model of bubble evolution with experimental observation for a lipid coated bubble. However, the elasticity model merits scrutiny; from Eq. (5), one notes $E^s \approx \Delta\gamma / (\Delta A/A)$, where A is the equivalent area per surfactant molecule, as indeed used in static interfacial measurements. One can estimate $\Delta\gamma \sim 0.07$ N/m (if one assumes that the surface tension goes to zero upon adsorption of lipids). Therefore, for $E^s \sim 1$ N/m, one has to have corresponding $\Delta A/A \sim 10^{-2}$. However, the value that can be estimated from Fig. 1 of the paper by Marmottant et al. [41] is much larger, of the order $\Delta A/A \sim 0.5$; one estimates from this figure $E^s \sim 0.12$ N/m. Indeed, Langmuir trough measurements (such as the one presented in Fig. 1 of the paper [41]) have produced low values of surface elasticity. Li et al. measured surface elasticity of a DPPC monolayer using a transient drop relaxation method as well as an oscillating barrier in a Langmuir trough,

and found $E^s = 0.01$ – 0.07 N/m [42]. They surmised the highest value to be for a solid layer. On the other hand, from acoustic attenuation measurements, $E^s \sim 0.5$ N/m was inferred for contrast agent Sonavue, a value similar to our own estimation for Sonazoid [43]. Goertz et al. found $E^s \sim 0.76$ – 0.86 N/m for Definity again using attenuation at 10–30 MHz [44]. Zong et al. used a mixture of two surfactants, Span60 and Tween80 at different compositions to create encapsulated microbubbles [45]. They measured interfacial elasticity $E^s = 0.013$ – 0.036 N/m using Langmuir trough for a monolayer made of the two components. However, they used $E^s = 0.5$ – 4 N/m for their simulation to match with experimentally measured subharmonic response from encapsulated bubbles. From this brief review of the literature, we conclude that measurement using a Langmuir trough gives rise to a lower value than what is needed to match acoustic experiments. A partial explanation can be found by noting that the surface elasticity depends on the frequency. Attenuation and bubble oscillations are performed at MHz frequency—as a function of frequency, complex materials show higher elasticity at higher frequencies. Also one should note that once the interface becomes solid-like there can be an order of magnitude increase in elasticity value. Using a Langmuir trough, He et al. showed that for a stearic acid monolayer at a very high compression of stearic acid molecules, surface elasticity increases from 0.079 N/m to 5.0 N/m [46]. They surmised that at such high compression, the surfactant layer behaves like a two-dimensional crystalline solid. In light of this discussion, we feel that for the gas transport process of concern here, the surface is probably in a liquid state with low value of surface elasticity, and only at the last stage of maturation, it might reach a solid phase. During this process the surface elasticity value is of the same order as that of surface tension $E^s \sim \gamma_0$. We use a value $E^s = 0.04$ N/m which is consistent with the Langmuir trough measurements mentioned above. It is higher than $\gamma_0 = 0.025$ N/m for a stable bubble in an air saturated medium. This value is much lower than what will be effective under high frequency oscillation of an already matured contrast microbubble. In any event, effect of the surface elasticity variation on the bubble evolution is also presented below.

3.2. Air bubble

First we investigate an air bubble of initial diameter 2.5 μ m with properties noted in Table 1. In Figs. 1–3, the bubble radius is plotted as a function of time for saturated ($f = 1$), unsaturated ($f = 0$) and oversaturated ($f = 1.5$) medium, respectively. The curves are plotted for different values of E^s/γ_0 . For $f = 1$ (Fig. 1), an encapsulated microbubble attains a long term non-zero radius only when $E^s/\gamma_0 > 1$. When this condition is satisfied, the bubble initially shrinks giving

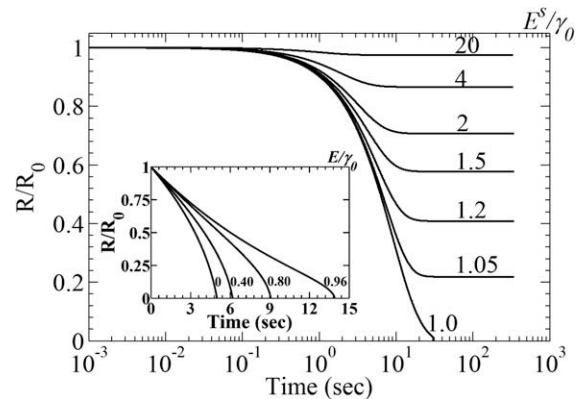


Fig. 1. Effect of interfacial elasticity on the stability and dissolution of an encapsulated 2.5 μ m diameter air bubble in an air saturated medium ($f = 1$). Numerical solution asymptotically matches the analytical equilibrium radius.

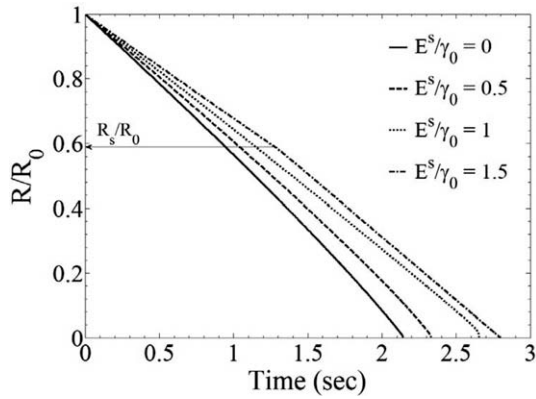


Fig. 2. Effect of interfacial elasticity on the dissolution of an encapsulated 2.5 μm diameter air bubble in a degassed medium ($f = 0$).

rise to a compressive stress that counterbalances the surface tension, and it then reaches the equilibrium value $R_{\text{equilibrium}}$ obtained analytically in (10). Fig. 1 shows that the limiting condition $E^s/\gamma_0 = 1$ results in a dissolution time $t_{\text{diss}}^{\text{limit}}$ which provides a time-scale of bubble stabilization for $E^s/\gamma_0 > 1$. The time to reach a stable radius for all values $E^s/\gamma_0 > 1$ is smaller than $t_{\text{diss}}^{\text{limit}}$. Increasing E^s/γ_0 decreases the time to reach stabilization. Also note that increasing E^s/γ_0 quickly reaches a saturation point of $R_{\text{stable}} = R_0$ beyond $E^s/\gamma_0 = 20$ (Fig. 1). For $E^s/\gamma_0 \leq 1$, a bubble dissolves within seconds (inset of Fig. 1) as the surface tension remains nonzero even though the compressive stress builds up with decreasing radius.

In Fig. 2, we consider the case of a degassed medium ($f = 0$), where undersaturation results in bubble dissolution as predicted by Eq. (7). For the case of $E^s \leq \gamma_0$, similar to Fig. 1, surface tension remains nonzero aiding the process of dissolution. For $E^s > \gamma_0$, dissolution is driven by surface tension ($\gamma(R) > 0$) and undersaturation for $R > R_s$ (shown by an arrow in Fig. 2). However, afterwards, for $R \leq R_s$, $\gamma(R) = 0$, and only undersaturation remains effective [see Eq. (8)]. Correspondingly the dissolution times in Fig. 2 are smaller than those in the saturated medium (Fig. 1). In Fig. 3 ($f = 1.5$) for $E^s > \gamma_0$, we obtain nonzero equilibrium radius as per Eq. (11). For $E^s \leq \gamma_0$, $f = 1.5$ satisfies the critical condition (12) for attaining an equilibrium radius. Accordingly, in Fig. 3, we obtain a stable radius for all values of E^s/γ_0 . Indeed for decreasing E^s/γ_0 , the equilibrium radius $R_{\text{equilibrium}}^{(1)}$ increases as per Eq. (12). Furthermore, for $E^s \leq \gamma_0$, we only obtain $R_{\text{equilibrium}}^{(1)}$ indicating that the other equilibrium solution $R_{\text{equilibrium}}^{(2)}$ is unstable.

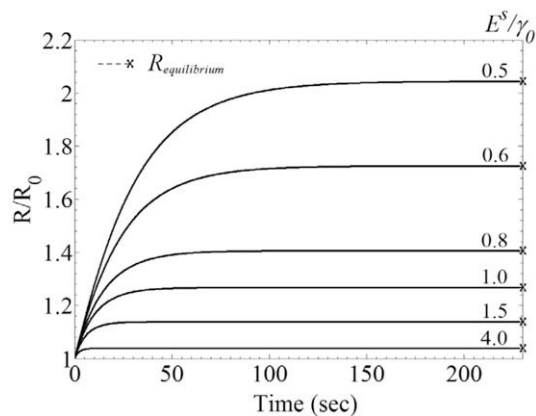


Fig. 3. Effect of interfacial elasticity variation on the growth of an encapsulated 2.5 μm diameter air bubble in an air oversaturated medium ($f = 1.5$). The value of f larger than the critical value for achieving an equilibrium radius. Numerical solution asymptotically matches the analytical equilibrium radius.

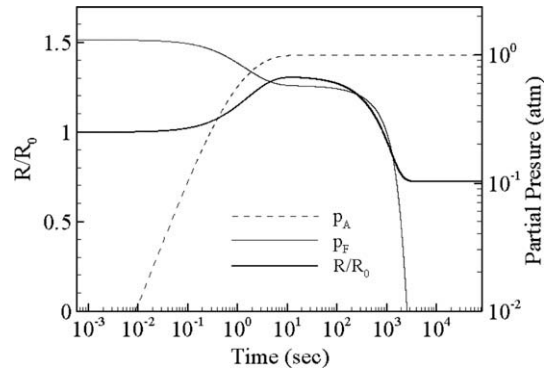


Fig. 4. Evolution of the radius of an encapsulated perfluorocarbon bubble of 2.5 μm diameter in the air-saturated medium ($f = 1$) for $E^s/\gamma_0 = 1.6$.

3.3. Perfluorocarbon bubble

We study a perfluorocarbon bubble of diameter 2.5 μm. In this section, we assume the medium to be saturated with air. Therefore, the surface tension controls the bubble behavior. In Fig. 4, we plot the time evolution of radius as well as air and perfluorocarbon pressures p_A and p_F for Definity bubble using $E^s \sim 0.04$ N/m ($E^s/\gamma_0 = 1.6$). With $E^s/\gamma_0 > 0$, a stable bubble is expected in the long-time limit. Initially because there is no air inside the bubble, air diffuses into the bubble. Air partial pressure rises sharply and reaches an equilibrium with outside pressure within few seconds. Air diffusivity being higher than that of OFP, the initial bubble behavior is essentially controlled by air diffusion. Therefore, the bubble grows due to air intake and reaches a maximum radius during air pressure equilibration. Such transient swelling of contrast microbubbles have been reported in experiments [24–27]. Afterwards OFP diffusion controls the bubble behavior, and the bubble radius reduces. But elastic stress in the encapsulation, resulting from the drop in radius below the stress-free value R_0 , counterbalances surface tension, leading finally to an equilibrium radius which is 61% of the initial radius. It takes ~ 3000 s to reach this state. At this point the bubble is an air bubble with OFP completely dispelled from the bubble.

In Fig. 5, we investigate a case of bubble dissolution resulting from $E^s/\gamma_0 = 0.4$ with other parameter values the same as that of Fig. 4. Similar to the previous case, the air pressure equilibrates quickly, and the bubble initially grows due to air ingress. But then in conformity with our analysis, the bubble dissolves due to outward diffusion of both air and OFP in ~ 1000 s. In the final phase of dissolution, the small radius of the bubble gives rise to a sharp increase in OFP pressure inside the bubble even though OFP

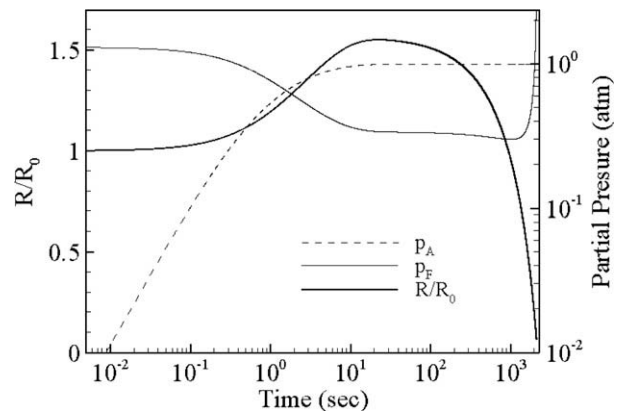


Fig. 5. Growth and dissolution behavior of an encapsulated perfluorocarbon bubble of 2.5 μm diameter in the air-saturated medium ($f = 1$) for $E^s/\gamma_0 = 0.4$.

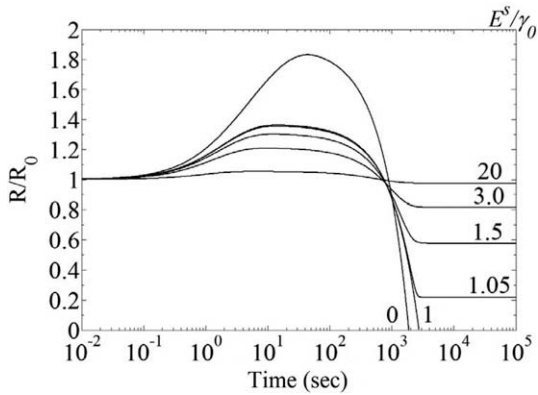


Fig. 6. Effect of interfacial elasticity variation on the dissolution of an encapsulated perfluorocarbon bubble of 2.5 μm diameter in air saturated medium ($f = 1$).

content decreases. This case of low elasticity models the case of a contrast microbubble with its encapsulation ruptured [24,47,48].

Next, we perform parametric studies varying several properties. Fig. 6 shows the effects of varying surface elasticity on bubble radius dynamics. As expected, for $E^s/\gamma_0 < 1$ a bubble dissolves, and for $E^s/\gamma_0 > 1$ it reaches a stable radius. The stable radius is the same as what we find for a pure air bubble as expected from our analysis in Section 2. We also note that increasing E^s also decreases the extent of transient increase in radius due to initial intake of air; increasing elasticity increases resistance towards both increase and decrease of bubbles. Notice also the quick saturation of the curves at higher value of E^s indicating that above $E^s/\gamma_0 \sim 20$, increasing E^s does not change the dynamics. Fig. 7 shows a parametric study with variation in gas permeability through the encapsulation. Both air and OFP permeabilities are varied by the same factor. Maximum bubble radius, final bubble radius and the growth and dissolution pattern are found to be independent of permeability. However, lower permeability expectedly slows the dynamics; the bubble reaches the long-term stable value at a later time. In Fig. 8, the curves for different permeabilities collapse on to a single curve when time is scaled by permeability indicating that R_0/h_g is the proper time scale of the problem. In the inset, we show that the time t_{stable} to reach the stable radius varies linearly with permeability.

In a typical contrast agent such as Definity, variation in octafluoropropane content and radius is expected. Fig. 9 shows the effect of initial mole fraction X_F of OFP on bubble radius evolution. The final equilibrium value of radius does not depend on X_F , because by this time all OFP is dispelled form the bubble. However, the time to reach equilibrium decreases with increasing X_F . Due

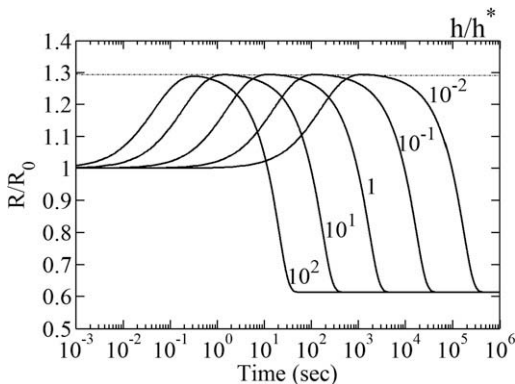


Fig. 7. Growth and dissolution behavior of an encapsulated 2.5 μm diameter perfluorocarbon microbubble in the air saturated medium for different permeability values, $h_a^* = 2.857 \times 10^{-5}$ m/s, $h_f^* = 1.6 \times 10^{-6}$ m/s.

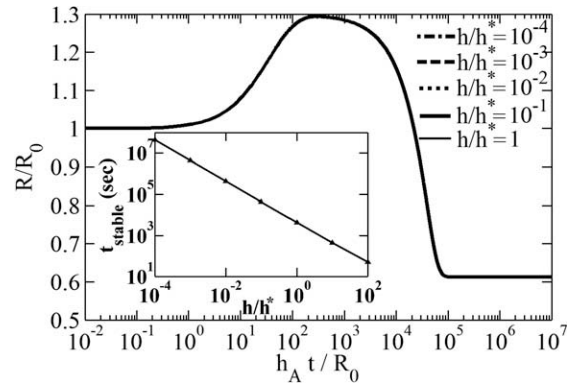


Fig. 8. Variation of relative encapsulated bubble radius with nondimensionalized time for different permeabilities of the encapsulation, and variation of t_{stable} with encapsulation permeability in the inset, $h_a^* = 2.857 \times 10^{-5}$ m/s, $h_f^* = 1.6 \times 10^{-6}$ m/s.

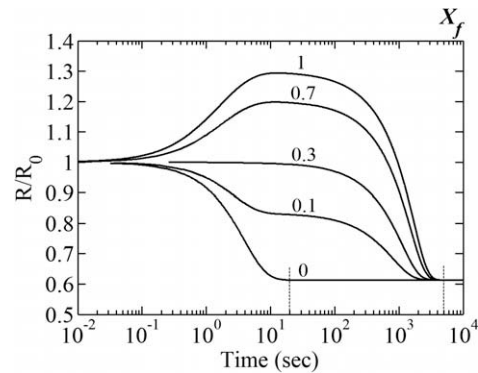


Fig. 9. Effect of initial mole fraction on the growth and dissolution behavior of an encapsulated 2.5 μm diameter perfluorocarbon microbubble in an air saturated medium.

to the higher air diffusivity, an air bubble ($X_F = 0$) shrinks down to its final radius within 20 s. On the other hand, initial presence of OFP in the bubble leads to a transient rise before reaching the stable state. The time to reach the stable state t_{stable} is two orders of magnitude higher than that of the air bubble. t_{stable} is independent of the initial mole fraction of OFP beyond a value of 10%. Fig. 10 shows the effect of initial radius on bubble evolution. We note from Eq. (10) that for saturated medium ($f = 1$), the normalized equilibrium radius does not depend on initial radius. However, larger initial radius leads to larger relative radius during

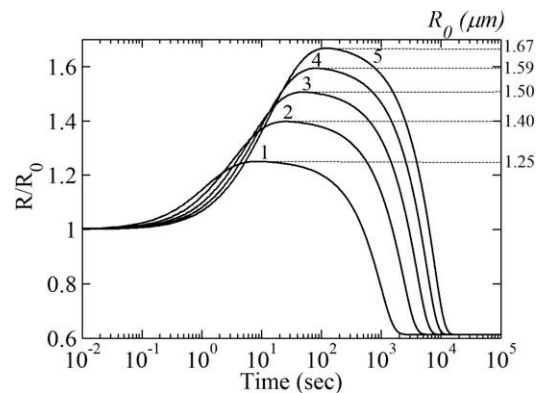


Fig. 10. Effect of initial bubble radius on the growth and dissolution behavior (R/R_0 vs. t) of an encapsulated 2.5 μm diameter perfluorocarbon microbubble in an air saturated medium.

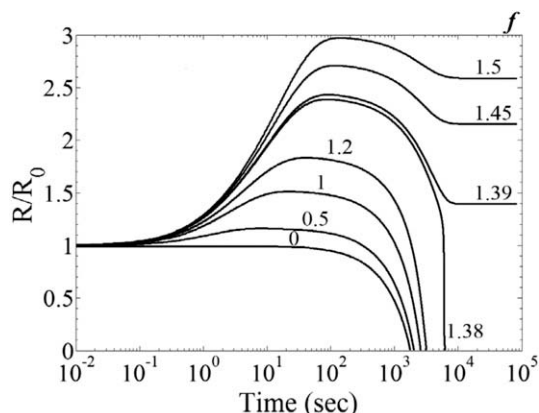


Fig. 11. Effect of saturation level of the surrounding medium on the growth and dissolution behavior of an $2.5\ \mu\text{m}$ diameter encapsulated perfluorocarbon microbubble ($E^s = 0.4\gamma_0$).

transient, and correspondingly takes longer time to reach the long-time equilibrium.

Finally, we investigate the effects of saturation on a perfluorocarbon bubble with a weakly elastic encapsulation, $E^s = 0.4\gamma_0$, and therefore nonzero $\gamma(R)$ for all values of radius (Fig. 11). For this case of $E^s/\gamma_0 < 0$, Eq. (12) predicts a critical saturation level $f^{\text{critical}} = 1.38678$ above which the bubble reaches equilibrium radius $R_{\text{equilibrium}}^{(1)}$; the oversaturation overcomes the dissolving force of the surface tension. Indeed, we find that for $f < f^{\text{critical}}$ the bubble dissolves, but $f > f^{\text{critical}}$ the bubble reaches the equilibrium value.

4. Conclusion

We investigate the effects of encapsulation elasticity on dissolution and stabilization of encapsulated contrast microbubbles using a mathematical model. An interfacial rheological model using a surface dilatational elasticity is used to describe the encapsulation. We show that encapsulation elasticity can stabilize a contrast microbubble against diffusion driven dissolution. We obtain explicit analytical condition between surface tension and the surface dilatational elasticity that needs to be satisfied for achieving long-time non-zero bubble radius. The condition varies with the level of saturation of the outside medium—undersaturation results in eventual bubble dissolution for all encapsulations while higher level of saturation impedes dissolution. We also account for the presence of a perfluorocarbon gas inside contrast microbubble and dissolved air outside. We then investigate an encapsulated octafluoropropane-filled microbubble with the physical properties representative of the lipid-coated Definity contrast agent. With a surface dilatational elasticity of $0.04\ \text{N/m}$ and surface tension of $0.025\ \text{N/m}$, it obtains a stable non-zero radius in the long-time limit in an air-saturated medium. The bubble experiences a transient growth before settling down to a radius 60% of the initial radius over a time scale of 3000 s. Increasing elasticity increases long-time equilibrium radius, with a saturation of the effects at higher values. Variations in initial mole fraction of octafluoropropane, initial radius and encapsulation permeability do not change the final value of the equilibrium radius normalized by its initial value. But they affect the time scale of the evolution. Larger initial radius results in larger transient swelling. For a weakly elastic encapsulation, air saturation of the surrounding medium above a critical value results in a stable bubble.

Acknowledgments

The authors acknowledge support from NSF CBET-0651912. It is also partially supported by US Army Medical Research Material Command under W81XWH-08-1-0503, AHA Grant Nos. 06554414 and NIH HL081892.

Appendix A. Supplementary data

Supplementary data associated with this article can be found, in the online version, at [doi:10.1016/j.jcis.2009.05.019](https://doi.org/10.1016/j.jcis.2009.05.019).

References

- [1] N. deJong, L. Hoff, T. Skotland, N. Bom, *Ultrasonics* 30 (1992) 95–103.
- [2] N. deJong, F.J. TenCate, *Ultrasonics* 34 (1996) 587–590.
- [3] K. Ferrara, R. Pollard, M. Borden, *Annu. Rev. Biomed. Eng.* 9 (2007) 415–447.
- [4] K. Ferrara, *J. Nucl. Med.* 48 (2007) 22N.
- [5] A.L. Klibanov, *Invest. Radiol.* 41 (2006) 354–362.
- [6] A.L. Klibanov, *Adv. Drug Delivery Rev.* 37 (1999) 139–157.
- [7] R.E. Pollard, T.C. Garcia, S.M. Stieger, K.W. Ferrara, A.R. Sadlowski, E.R. Wisner, *Invest. Radiol.* 39 (2004) 340–349.
- [8] R.J. Price, D.M. Skyba, T.C. Skalak, S. Kaul, *Circulation* 98 (1998) 570.
- [9] R.V. Shohet, S.Y. Chen, Y.T. Zhou, Z.W. Wang, R.S. Meidell, T.H. Unger, P.A. Grayburn, *Circulation* 101 (2000) 2554–2556.
- [10] K. Sarkar, P. Jain, A. Katiyar, *Ultrasound Med. Biol.* (2009), [doi:10.1016/j.ultrasmedbio.2009.04.010](https://doi.org/10.1016/j.ultrasmedbio.2009.04.010).
- [11] P.S. Epstein, M.S. Plesset, *J. Chem. Phys.* 18 (1950) 1505–1509.
- [12] W.H. Wang, C.C. Moser, M.A. Wheatley, *J. Phys. Chem.* 100 (1996) 13815–13821.
- [13] M.A. Borden, M.L. Longo, *Langmuir* 18 (2002) 9225–9233.
- [14] N. deJong, L. Hoff, *Ultrasonics* 31 (1993) 175–181.
- [15] N. deJong, R. Cornet, C.T. Lancee, *Ultrasonics* 32 (1994) 447–453.
- [16] C.C. Church, *J. Acoust. Soc. Am.* 97 (1995) 1510–1521.
- [17] L. Hoff, P.C. Sontum, J.M. Hovem, *J. Acoust. Soc. Am.* 107 (2000) 2272–2280.
- [18] D. Chatterjee, K. Sarkar, *Ultrasound Med. Biol.* 29 (2003) 1749–1757.
- [19] K. Sarkar, W.T. Shi, D. Chatterjee, F. Forsberg, *J. Acoust. Soc. Am.* 118 (2005) 539–550.
- [20] K.E. Morgan, J.S. Allen, P.A. Dayton, J.E. Chomas, A.L. Klibanov, K.W. Ferrara, *IEEE Trans. Ultrason. Ferroelect. Freq. Control* 47 (2000) 1494–1509.
- [21] D.B. Khismatullin, A. Nadim, *Phys. Fluids* 14 (2002) 3534–3557.
- [22] S. Hilgenfeldt, D. Lohse, M. Zomack, *Eur. Phys. J. B* 4 (1998) 247–255.
- [23] P.B. Duncan, D. Needham, *Langmuir* 20 (2004) 2567–2578.
- [24] D. Chatterjee, P. Jain, K. Sarkar, *Phys. Fluids* 17 (2005) 100603.
- [25] W.S. Chen, T.J. Matula, L.A. Crum, *Ultrasound Med. Biol.* 28 (2002) 793–803.
- [26] J.F. Guan, T.J. Matula, *J. Acoust. Soc. Am.* 116 (2004) 2832–2842.
- [27] W.T. Shi, F. Forsberg, *Ultrasound Med. Biol.* 26 (2000) 93–104.
- [28] J.S. Darrigo, T. Imae, *J. Colloid Interface Sci.* 149 (1992) 592–595.
- [29] D.E. Yount, *J. Acoust. Soc. Am.* 65 (1979) 1429–1439.
- [30] W. Kloeck, T. van Vliet, M. Meinders, *J. Colloid Interface Sci.* 237 (2001) 158–166.
- [31] M. Blank, V.K. La Mer, The energy barrier for monolayer penetration, in: V.K. La Mer (Ed.), *Retardation of Evaporation by Monolayers*, Academic Press, New York, 1962, pp. 59–66.
- [32] E. Lac, D. Barthes-Biesel, N.A. Pelekasis, J. Tsamopoulos, *J. Fluid Mech.* 516 (2004) 303–334.
- [33] A. Kabanov, D. Klein, T. Pelura, E. Schutt, J. Weers, *Ultrasound Med. Biol.* 24 (1998) 739–749.
- [34] V. Sboros, C.M. Moran, S.D. Pye, W.N. McDicken, *Ultrasound Med. Biol.* 27 (2001) 1367–1377.
- [35] E. Quaia, Classification and safety of microbubble-based contrast agents, in: E. Quaia (Ed.), *Contrast Media in Ultrasonography: Basic principles and Clinical Applications*, Springer, Berlin, 2005, pp. 3–14.
- [36] D.H. Kim, M.J. Costello, P.B. Duncan, D. Needham, *Langmuir* 19 (2003) 8455–8466.
- [37] M. Blank, *Fed. Proc.* 21 (1962) 151.
- [38] M. Blank, *J. Phys. Chem.* 68 (1964) 2793.
- [39] M.A. Borden, M.L. Longo, *J. Phys. Chem. B* 108 (2004) 6009–6016.
- [40] M.A. Borden, G.V. Martinez, J. Ricker, N. Tsvetkova, M. Longo, R.J. Gillies, P.A. Dayton, K.W. Ferrara, *Langmuir* 22 (2006) 4291–4297.
- [41] P. Marmottant, S. van der Meer, M. Emmer, M. Versluis, N. de Jong, S. Hilgenfeldt, D. Lohse, *J. Acoust. Soc. Am.* 118 (2005) 3499–3505.
- [42] J.B. Li, G. Kretschmar, R. Miller, H. Mohwald, *Colloids Surf. A* 149 (1999) 491–497.
- [43] J.M. Gorce, M. Arditi, M. Schneider, *Invest. Radiol.* 35 (2000) 661–671.
- [44] D.E. Goertz, N. de Jong, A.F.W. van der Steen, *Ultrasound Med. Biol.* 33 (2007) 1376–1388.
- [45] Y.J. Zong, M.X. Wan, S.P. Wang, G.L. Zhang, *Ultrasonics* 44 (2006) E119–E122.
- [46] P.S. He, K. Fang, G. Zou, J.P.K. Peltonen, J.B. Rosenholm, *Colloids Surf. A* 201 (2002) 265–273.